第 34 卷第 8 期 无 机 化 学 学 报 Vol.34 No.8
2018 年 8 月 CHINESE JOURNAL OF INORGANIC CHEMISTRY 1517-1530

兼具抗癌和药物递送作用的硒掺杂羟基磷灰石微球

王艳华*,[1] 郝 颃[2] 巫剑雄[1] 姚 媛[1] 覃 娜[1] 何文聪[3]
([1]三峡大学医学院,宜昌 443002)
([2]华中科技大学先进生物材料与组织工程研究中心,武汉 430074)
([3]三峡大学第一临床医学院,宜昌 443002)

摘要:利用碳酸钙作为处理模板,通过共沉淀联合水热法,制备了硒元素掺杂羟基磷灰石微球(HASe),期望硒掺杂能提高 HA 对溶菌酶的加载,并增强 HASe 微球的杀菌活性。所合成的 HASe 微球经 SEM、TEM、DLS、XRD、FTIR 和 TGA 测试对其理化性能进行了表征。并且利用姜黄素作为模式药物,评估了它们的药物加载及控释效能。结果发现,所合成的 HASe 产物为直径约 1.0 μm 的球体,球壁粘附有许多羟基磷灰石纳米棒(长约 150 nm、宽约 20 nm)。该 HASe 微球对姜黄素具有高的药物加载和缓慢稳定的控释效应。其药物加载量为(88.72±0.01) mg·g^{-1},在 0~159 h 内仅有不到 1.5 mg 的姜黄素被释放,且无爆释现象。此外,还通过血液分析和细胞实验评估了 HASe 微球的毒性行为。与无硒 HA 微球相比,HASe 微球的血液毒性低,对细胞损伤少,然而对骨肉瘤细胞生长却具有强的抑制作用。

关键词:羟基磷灰石;硒;中空微球;药物递送系统;姜黄素
中图分类号:TQ126.3 **文献标识码**:A **文章编号**:1001-4861(2018)08-1517-14
DOI:10.11862/CJIC.2018.199

Enhanced Antitumor Effect and Drug Delivery from Se Doped Hydroxyapatite Microspheres

WANG Yan-Hua*,[1] HAO Hang[2] WU Jian-Xiong[1] YAO Yuan[1] QIN Na[1] HE Wen-Cong[3]
([1]*Medical College of China Three Gorges University, Yichang, Hubei* 443002, *China*)
([2]*Advanced Biomaterials and Tissue Engineering Center, Huazhong University of Science and Technology, Wuhan* 430074, *China*)
([3]*The First College of Clinical Medical Science, China Three Gorges University, Yichang* 443002, *China*)

Abstract: Selenium doped hydroxyapatite microspheres (HASe) were prepared by using self-sacrificing $CaCO_3$ as template via hydrothermal route, and their physicochemical properties were characterized by SEM, TEM, DLS, XRD, FTIR and TGA. The curcumin was employed as the model drug, and its delivery behavior from HASe microspheres was evaluated with the loading efficacy and controlled-release efficiency. As a result, it was observed that the synthetic HASe products are spherical with an average diameter of about 1.0 μm. The surface of the microspheres is constructed by subtle units of hydroxyapatite nanorods which are 150 nm in length and 20 nm in width. HASe microspheres exhibit a high drug loading efficacy and slowly sustainable release behavior for curcumin. The loading amount of HASe10 was (88.72±0.01) mg·g^{-1}, and less than 1.5 mg of curcumin was released from it during 0~159 h. There is no burst release but slow sustainable release manner in it. Moreover, the toxicity of HASe microspheres was investigated by blood assay and cell experiment. Compared with selenium-free HA microspheres, HASe microspheres show lower blood toxicity to healthy man, and less damage to normal cells, but stronger inhibition on the growth of the osteosarcoma cells.

Keywords: hydroxyapatite; selenium; hollow microspheres; drug delivery system; curcumin

收稿日期:2018-02-11。收修改稿日期:2018-06-07。
国家自然科学基金(No.81602559)资助项目。
*通信联系人。E-mail:wangyanhua@ctgu.edu.cn,Fax:+86-717-6397198

0 Introduction

The therapy of osteosarcoma is still far from satisfactory due to the high tumor relapse postoperatively. Hence, it is imperative to develop new therapeutic strategies. Hydroxyapatite ($Ca_{10}(PO_4)_6(OH)_2$, HA) is the main component of human bones and teeth[1], and has been widely applied in various biomedical fields such as bone repair and tissue engineering[2-3], anticancer therapy[4-5], and drug delivery[6-8]. In recent decades, HA has been tremendously studied as bone matrix material and drug carriers, targeting the rapid bone repair, high bactericidal and antitumor effect[9-11]. Benedetti used the hydroxyapatite nanocrystals to adsorb cisplatin, and got increased antitumor efficacy for HeLa, MCF-7 and HS-5 cell lines[12]. In our previous study, the HASe nanocarrier, with high loading capacity and biologic activity, was applied to deliver lysozyme to the infectious sites[13]. Except for HA-nanocarrier, HA-micron scale particles, because of the large specific surface area and high loading capacity, are also good candidates to deliver doxorubicin hydrochloride (DOX) to kill the cancerous cells[14]. Kamitakahara prepared micrometer-sized composites of magnetic HA nanoparticles via hydrothermal process, and found these particles generate sufficient heat energy under an alternating magnetic field, thus killing bone tumor cells[10]. Regardless of morphology and size, HA is of great potential served as carriers for drug delivery in the therapy of tumors[15-18].

Selenium (Se) is a trace mineral element with various biological effects, especially in the aspect of bone remodel and growth. Se also has strong anticancer activity on various types of carcinoma. Dual-functional selenium substituted hydroxyapatite nanoparticles (HASe) were synthesized in our lab[19]. Good results were obtained in the treatment of osteosarcoma-related bone defect[20]. Besides, it was reported that the doped selenium improves the loading efficacy of HA lattice for lysozyme, as well as changes the release fashion[13]. For broadening the range of biomedical applications of HASe particles in our group, the hollow porous HASe microspheres were fabricated to enhance the anticancer effect on osteosarcoma. Many literatures provided various strategies to synthesize this type of microspheres[21-28]. One of these methods is the template assisted route. For example, HA nanorod-assembled porous hollow polyhedra can be successfully prepared at room temperature with a self-sacrificing $Ca(OH)_2$ template, which shows increased bone regenerative capability for bone defect[23]. Ma et al. prepared nanostructured porous hollow ellipsoidal capsules of HA using $CaCO_3$ templates[29]. Ye et al. prepared HA hollow nanospheres using poloxamer (Pluronic P123) and polysorbate 60 (Tween 60) micelles as templates[30]. Qi et al. prepared nanosheet-assembled porous hollow microspheres of HA using DNA molecules as templates by the hydrothermal method[31]. Eventually, they all present good biologic effects. However, it remains a challenge to prepare micro-structured porous hollow element doped HA materials by the simple, rapid, and environmentally friendly template route, which presents good selectivity and high stability for the loaded drug.

HASe nanocarrier has been developed in our lab[19], and has showed good drug loading and release property, but the fine structure and function of HASe microcarrier has not been studied yet. In this work, the template-hydrothermal route was used to fabricate HASe microspheres by synthetic vaterite $CaCO_3$ as the sacrificial template. The as-prepared HASe microspheres were explored for potential application in drug-loading and controlled-release. Curcumin (Cur), a traditional Chinese medicine, was selected as a model drug, owing to the famous broad-spectrum anti-cancer properties on various type of cancers[32-35]. The HASe-Cur delivery system shows high loading efficiency, sustainable slow-release, low blood toxicity and high anticancer effect on the growth of bone tumor cells. So, it is feasible to use the HASe microsphere as new microcarrier to deliver anticancer drugs, especially in the oncotherapy of osteosarcoma.

1 Experimental

1.1 Materials

Poly (styrene sulfonic acid) sodium salt (PSS,

powder, M_r=70 000, Shanghai Jianglai Biotechnology Corporation, China), Cur (Shanxi Huike Chemical Reagent Corporation, China), sodium selenite (Na_2SeO_3, Micxy Reagent Company, China), calcium chloride ($CaCl_2$, 99%, National Medicine Chemical Reagent Company, China), sodium carbonate (Na_2CO_3, 99.8%, Shanghai Hongguang Chemical Reagent Factory, China), disodium hydrogen phosphate (Na_2HPO_4, 99.99%, Wuhan Chemical Reagent Factory, China), sodium hydroxide (NaOH, 99%, National Medicine Chemical Reagent Company, China), hydrochloric acid (HCl, Shanghai Sanying Chemical Reagent Co., Ltd.), ethanol (≥99.7%, Hangzhou Gaojing Fine Chemical Industry Co., Ltd.), and phosphate buffer saline (pH= 7.2 ±0.2) were obtained commercially, and used as received without further purification. All other reagents of chemical grade or above were used as provided.

1.2 Preparation of $CaCO_3$ template

The $CaCO_3$ template was synthesized according to the strategies reported by the references[14,26]. PSS was used as a regulation template of the reactant aqueous solution at room temperature. Briefly, the $CaCl_2$ solution (10 mL, 0.2 mol·L^{-1}) was poured into PSS (100 mL, 10 mg·mL^{-1}) solution under vigorous magnetic agitation, and then the Na_2CO_3 solution (10 mL, 0.2 mol·L^{-1}) was added dropwise into the above mixed solution under vigorous magnetic stirring to obtain a white suspension. After the complete addition, the white suspension was agitated continuously at room temperature for 2 h, and then followed by centrifugation (4 000 r·min^{-1}, 15 min), washed three times with distilled water and absolute ethanol respectively, and finally dried at 60 ℃ for 48 h.

1.3 Preparation of HASe microspheres from $CaCO_3$ template

The HASe microspheres were prepared by an anion-exchange process using the previously prepared $CaCO_3$ as the sacrificial template in a hydrothermal method. Specific operation referred to the reported literature with minor modification[14]. In a typical experiment for HASe10 sample, 100 mL of the P and Se mixed solution contained 14.2 mg·mL^{-1} Na_2HPO_4 and 0.1 mg·mL^{-1} Na_2SeO_3 was added into 0.2 g of the $CaCO_3$. The pH value of the resulting suspension was adjusted to 11.0 using 1 mol·L^{-1} NaOH solution. The suspension was transferred into a Teflon-lined stainless steel autoclave, sealed, and heated by a hydrothermal method at 120 ℃ for 45 min under 0.1 MPa of atmosphere pressure. At the end of hydrothermal reaction, the product was collected by centrifugation, washed three times with distilled water and absolute ethanol respectively, and dried at 60 ℃ for 48 h. The powder was stored in vacuum for the further studies. For the fabrication of selenium-free HA and selenium-doped HASe30 microspheres, the clear Na_2HPO_4 solution (14.2 mg·mL^{-1}, 100 mL), and 100 mL of the P and Se mixed solution contained 14.2 mg·mL^{-1} Na_2HPO_4 and 0.3 mg·mL^{-1} Na_2SeO_3, were added into 0.2 g of the $CaCO_3$ powders, respectively.

1.4 Characterization

The morphology and size of the as-synthesized samples were characterized by field emission scanning electron microscopy (FE-SEM) (Nova nanoSEM 450, FEI, Netherlands), transmission electron microscopy (TEM) (Tecnai G220, FEI, Netherlands). The samples were ultrasonically dispersed in double distilled water and the size distribution of the samples was characterized by dynamic light scattering (DLS) (Nano-ZS90, Malvern, MA, USA). The crystalline phases of samples were examined with X-ray powder diffraction (XRD) (X′Pert PRO, PANalytical B.V. Co, Netherlands) using a monochromatic Cu $K\alpha$ radiation (λ=0.154 06 nm, 40 mA, 40 kV) in the 2θ range of 10°~70° with a step size of 0.02° per second. Fourier transform infrared spectra (FTIR) (NEXUS, Thermo Electron, USA) were collected at room temperature by using the KBr squash technique, working in the wavenumber range of 4 000 ~400 cm^{-1} with a resolution of 4 cm^{-1}. Thermogravimetric analysis (TGA) was conducted on a thermo-gravimetric analyzer (Diamond, PerkinElmer Instruments, USA) heated to 800 ℃ with a rate of 10 ℃·min^{-1} under nitrogen atmosphere.

1.5 *In vitro* materials degradation

For the *in vitro* degradation experiment, 50 mg samples were immersed in 10 mL phosphate buffered saline (PBS, pH 3.5 or 10.5), and constantly stirred in

a shaking bath at 37 ℃. At pre-determinant time intervals, 1 mL of the supernatant was withdrawn by centrifugation and replaced by the same volume of fresh medium. The concentration of calcium ions and selenium ions in the supernatant was measured by UV-Vis spectrophotometer (Nanoquant infinite M200 PRO, Tecan) at a wavelength of 612 and 365 nm, respectively, and calculated by using a standard calibration curve obtained under the same conditions. All the tests were carried out in triplicate and the average values were shown in this study.

1.6 Drug loading and *in vitro* drug release

The drug loading and *in vitro* drug release experiments were performed using Cur as a drug model. The procedure of Cur loading was performed as follows: 50 mg of sample was blended into Cur solution (5 mL, 1 mg·mL^{-1}) over 72 h under gentle shaking at 37℃. Then, the Cur-loaded particles were collected by centrifugation, and then dried in vacuum at 60 ℃ for 48 h. The amount of Cur in the supernatant was measured by UV-Vis spectrophotometer at a wavelength of 430 nm and calculated via a calibration curve. The amount of Cur encapsulated in the samples can be calculated by subtracting the amount in the supernatant from the initial dose. Therefore, the drug loading amount (DLA) in the final products was estimated by the following equation: $DLA=(w_a-w_s)/w_c\times100\%$, where w_a is the amount of Cur added to the reaction, w_s is the amount of Cur presented in the supernatant, w_c is the amount of obtained final dried products. The drug entrapment efficiency (DEE) was calculated by using the equation: $DEE=(w_a-w_s)/w_a\times100\%$.

For the *in vitro* drug release experiment, the Cur-loaded HA samples (5 mg) were immersed in 15 mL PBS with pH value equal to 7.2±0.2 under magnetic stirring at a constant rate of 150 r·min^{-1} at 37 ℃. The sample (1 mL) was removed at given time intervals for UV-Vis analysis and replaced by the same volume of fresh medium. The adsorption data ($OD_{430\,nm}$) were representative as the mean value of three parallel measurements.

1.7 Hemolysis test

For the hemolysis evaluation, the whole blood of forty healthy individuals was collected from the first college of clinical medical science of China Three Gorges University, and confirmed in the normalcy via blood-routine test. For the hemolysis analysis, 10 mg of each sample was resolved in 10 mL PBS (pH 7.2), and dispersed by ultrasonic for 20 minutes, then 20 μL of the above sample was added into 1mL human whole blood, thereafter incubated in 37℃ for 15 minutes, and finally the changes of the whole blood was monitored via blood routine test by blood analyzer (Mindray BC-1800, China). And the increase of the hemoglobin quantity in the blood could reflect the strong hemolytic toxicity of the materials.

1.8 Cytotoxicity assay

The human osteosarcoma SOSP-9607 cell and normal macrophages RAW-264.7 cell were used to test the cytotoxic effect of these microspheres. The human osteosarcoma SOSP-9607 cell lines were provided from the 4th military medical university, Xi′an, Shaanxi, China. The macrophages RAW-264.7 cell lines were provided from the Chinese Medicine Pharmacology Level 3 Laboratory of National Chinese Medicine Administrator at China Three Gorges University. The cancerous SOSP-9607 cell and normal RAW-264.7 cells were respectively cultured in RPMI 1640 medium and high glucose DMEM medium, supplemented with 10% fetal bovine serum in the 5% (*V*/*V*) CO_2, saturated humidity, 37 ℃ incubator (Sanyo CO_2 incubator, Japan). MTT test was used to monitor the cytotoxicity of the microspheres. Briefly, 1×10^4 cells were implanted into 96 well cell plate, and after 24 h of pasting, 1 mg microspheres were added into the medium. At the pre-determined intervals, the MTT test was applied to evaluate the cytotoxicity of the biomaterials. Meanwhile, in order to observe the impact of the microspheres on the cell migration ability, 5×10^3 cells were implanted into twelve well cell plate, and 5 mg microspheres were added into the medium, and a line at the bottom of the plate was given by the head of a needle from 10 mL syringe. After co-cultured for 48 h, the cell density and migration effect were monitored under a light microscope after dyed by the Wright′s-Gimsa.

1.9 Statistical analysis

The data was exhibited via mean±SD values of six independent experiments. For the comparison between two groups, two-tailed student′s *t*-test was used to calculate the statistical significance of the experimental results. Comparisons among three groups were tested using analysis of variance. $*p<0.05$ was considered to indicate significant difference, and $**p<0.01$ was considered to be greatly significant.

2 Results and discussion

2.1 Characterization of $CaCO_3$ template

The morphology of the synthesized vaterite $CaCO_3$ was observed from the SEM (Fig.1a). It showed a uniform spherical morphology with the average diameter of 1.0 μm. The XRD patterns of the synthesized vaterite $CaCO_3$ (Fig.1b) revealed that all the diffraction peaks accord well with the vaterite phase (PDF No.15-0020). The results show that the addition of PSS can greatly control the formation of vaterite phase. Literatures have provided good explanation that, PSS, a crystal growth regulator, has the ability of accelerating the transformation of $CaCO_3$ particles from calcite to vaterite[36]. The functional groups in the synthesized vaterite $CaCO_3$ have been characterized by FTIR spectra. As shown in Fig.1c, two absorption bands located at 877 and 745 cm^{-1} are the characteristic peaks of CO_3^{2-}, which are assigned as carbonate out-of-plane deformation and in-plane deformation, respectively. The absorption band at 745 cm^{-1} is the typical carbonate band deformation in vaterite $CaCO_3$, which is consistent with the observation from XRD results (Fig.1b). The broad absorption bands located at 1 566 and 1 358 cm^{-1} are the characteristic peaks of carbonyl groups (C-O bonds). Lots of sharp absorption bands aggregated in the range of 1 000~1 250 cm^{-1} are attributed to PSS[14], implying that a small amount of PSS is adsorbed on the surface or trapped in the nanopores of the vaterite $CaCO_3$. The wide band located at 3 435 cm^{-1} corresponds to the adsorbed H_2O molecules. The results of FTIR indicate that, the functional groups of $CaCO_3$ are visible in the synthesized sample, which could provide the carboxylic group serving as interactive site to initiate the transformation of the $CaCO_3$ to HA during the hydrothermal process.

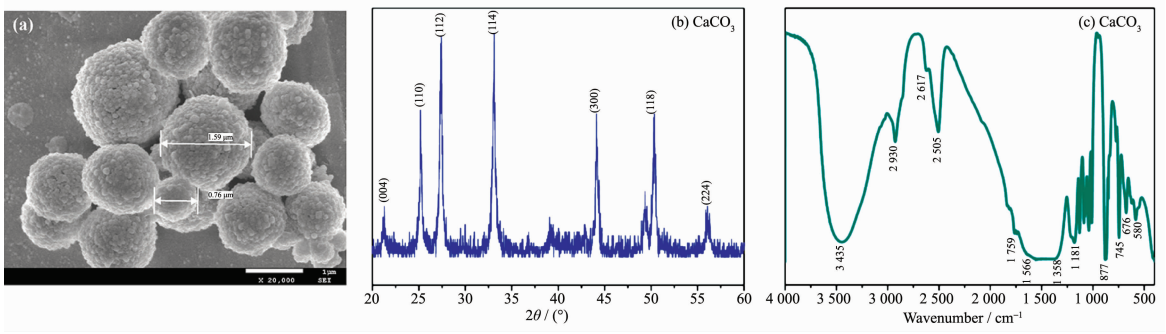

Fig.1　Characterization of $CaCO_3$ template: (a) SEM image; (b) XRD pattern (c) FTIR spectrum

2.2 Characterization of HASe microspheres

The morphologies of different HASe microspheres were confirmed by FE-SEM (Fig.2). The single dispersed spherical structure with cauliflower surface was apparent in the FE-SEM images of all samples. For HA microsphere, the wall was constructed with flake-like hydroxyapatite crystals, which distributed randomly and seemed to grow out of the center. For HASe10 microsphere, short clavite-like surface was visible. Such structure consisted of HA crystalline which arranges densely. For HASe30 microsphere, many flowerlike bundles were clearly observed. The microspheres with nano-flowers structure clustered together, but they were facilely distinguished from each other. Hydroxyapatite crystals grew from the center of the ball to the periphery, and constructed the fuzz-like surface. Such wispy crystals aligned precisely, which made the sphere present an urchin-like appearance.

As shown in Fig.3, the TEM images of HASe

microspheres exhibit a translucent center and a black edge, indicating that the synthetic microsphere has hollow structure. The wall of HASe microsphere was constructed by subtle units of hydroxyapatite nanorods

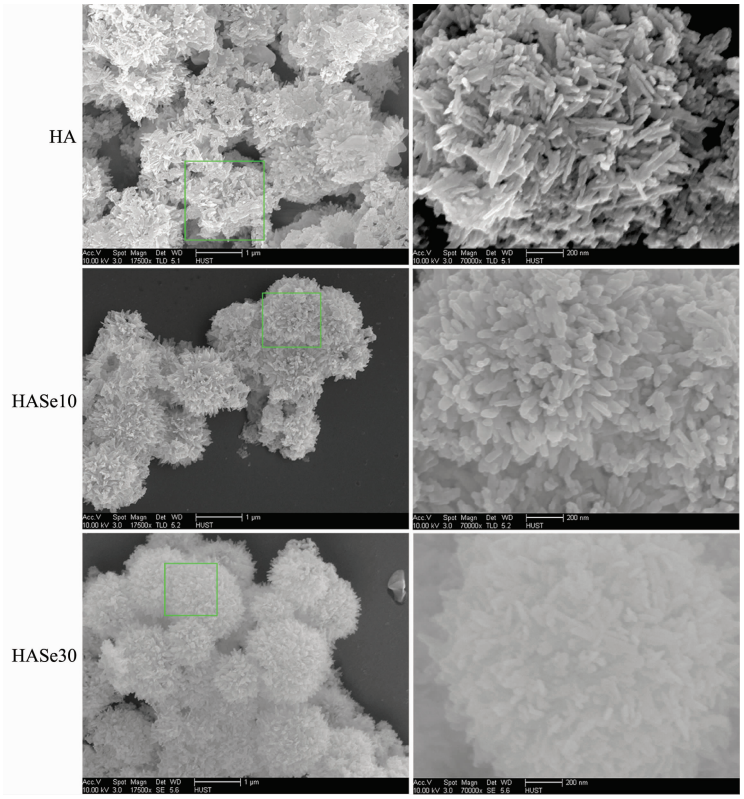

Right: the magnified picture of the grid of the left chart

Fig.2 Morphology characterization of HA and HASe microspheres

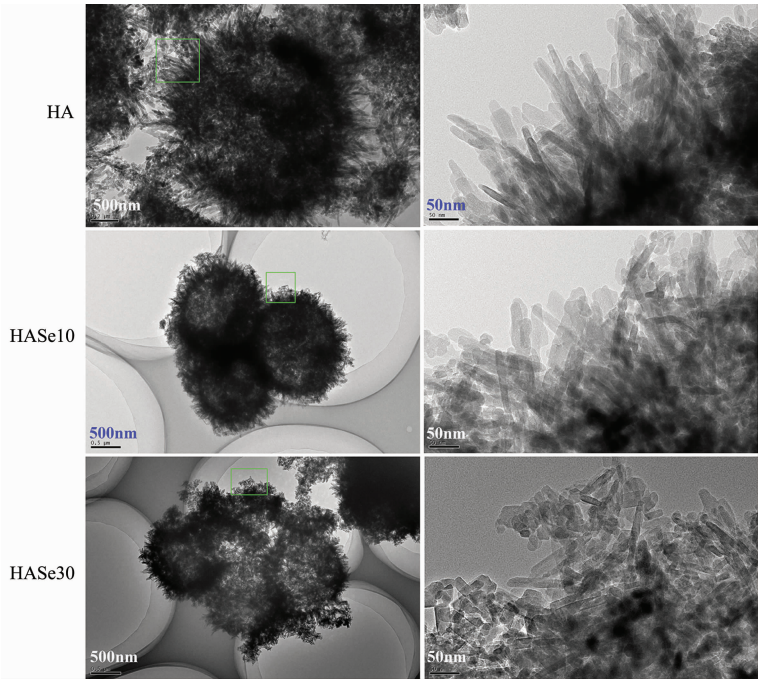

Right: the magnified picture of the grid of the left chart

Fig.3 TEM images of HA and HASe microspheres

with an average length of 150 nm and an average width of 20 nm. There were also small nuances among the three samples. Long nanorods units were shown in the HA group, whereas slightly short nanorods units were obtained in the HASe10 group. Most intriguing, some stubs and small brokens were shown on the wall of the HASe30 group. The formation of the nanorods units has greatly enlarged the surface area of the sphere, and such large interface provides a niche for them to interact with drug molecules, which is facilitated to increase the drug loading capacity.

The size of HASe microspheres were tested by dynamic light scattering (DLS), and the data are summarized in Table 1. The size of all samples was slightly larger via DLS measurement than SEM observations. In the SEM images, the HASe microspheres had a size distribution from 0.8 to 1.6 μm and the average diameter was about 1.0 μm. However, DLS measurements indicated that the size of the same sample was over 2.0 μm. The deviation stems from the fact that, as the DLS measurements provided the hydration size of microspheres, and all samples are dispersed in H_2O, there are inevitably some water molecules adsorbed on the surface of the microspheres, which increases the value of the sizes. Additionally, the size of HASe microspheres was slightly larger than that of the $CaCO_3$ template due to the formation of hydroxyapatite nanorods during the hydrothermal process. So, the surface of HASe microspheres become coarser than that of vaterite $CaCO_3$.

The XRD patterns of the HASe microspheres are presented in Fig.4a. All the peaks can be indexed and matched well with the hexagonal phase of hydroxyapatite (PDF No.09-0432), proving that hydroxyapatite is the main phase of the synthetic HASe microspheres. Hydrothermal fabrication is a successful route to prepare selenium doped HA microsphere with hydroxyapatite phase. As shown in the XRD patterns, the intensity of certain peaks increased with the increase of the dopant dose, which indicates the doped element could increase the crystallinity of the HA microspheres. In addition, certain peaks became broadened after doped. As shown in the inset of Fig.4a, the more selenium was doped into hydroxyapatite, the wider band of this plane is shown in the XRD pattern. The XRD results indicated that, the synthetic HASe microspheres are of the hydroxyapatite phase with better crystallinity, and selenium doping has no evident

Table 1　Size distribution of HA and HASe microspheres

Sample	Size / μm	Surface area / Volume / cm^{-1}
HA	2.493±0.014	61 443±25
HASe10	2.446±0.021	48 878±33
HASe30	3.381±0.015	42 798±29

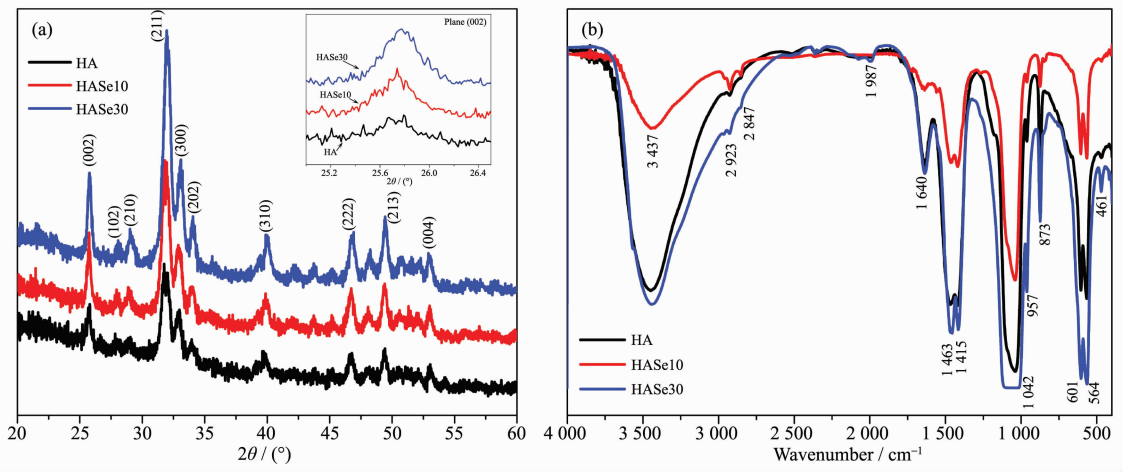

Inset: the magnification of the XRD patterns from 25° to 27°

Fig.4　(a) XRD patterns of HA and HASe microspheres; (b) FTIR spectra of HA and HASe microspheres

interference in the transformation from $CaCO_3$ to HA, which indicates the synthetic route was successful.

The functional groups in the HASe microspheres and the pure hydroxyapatite have been characterized by FTIR spectra. As shown in Fig.4b, the intense absorption band located at 1 042 cm^{-1} is ascribed to the stretching vibration (ν_3) of the phosphate (PO_4^{3-}) groups, and the absorption bands located at 564 and 601 cm^{-1} are attributed to the bending vibration (ν_4) of the PO_4^{3-} groups[19] The absorption bands located at 3 437 and 1 640 cm^{-1} are ascribed to the adsorbed water and hydroxyl group, respectively. In addition, the appearance of CO_3^{2-} absorption peaks at 873 cm^{-1} (ν_2), 1 415 and 1 463 cm^{-1} (ν_3) indicates the incorporation of CO_3^{2-} groups into hydroxyapatite lattice structure under the ambient atmosphere condition[13]. The FTIR results indicated that the synthetic HASe microspheres are the typical carbonated hydroxyapatite. Hydrothermal process could expedite the complete transformation of vaterite $CaCO_3$ into hydroxyapatite phase.

The HASe microspheres were subjected to thermal gravimetric analysis. Fig.5 shows the TG/DSC plots of all samples. The weight loss curves of the microspheres could be roughly divided into three steps. The initial weight loss from room temperature to 200 ℃ is due to the volatilization of physically adsorbed water. When the temperature arose from 200 to 500 ℃, the weight loss of about 4.86%, 3.30% and 3.11% in each curve was observed, which could be associated with the thermal decomposition of PSS, indicating that the polymer contents in HA, HASe10 and HASe30 microspheres are about 4.86%, 3.30% and 3.11%, respectively. At 500 ℃, the organic molecules were removed completely and only the HASe mineral microspheres were remained. There is still visible small weight loss, which might be ascribed to the decomposition of the carbonate groups substituted in the HA structure. According to the remained weight at 800 ℃, the mineral contents in the microspheres calculated from the TGA curve decreased from 21.12%, 13.49% to 11.82%, when the doped Na_2SeO_3 amount increased from 0 mg (HA), 10 mg (HASe10) to 30 mg (HASe30), respectively. Such changes further confirm the selenite ions substitute the carbonate groups of the HA structure, and the synthetic HASe microspheres are selenite-substituted-carbonate HA phase. The substitution mechanism involved is complex, and our previous work has provided detailed explanation[19].

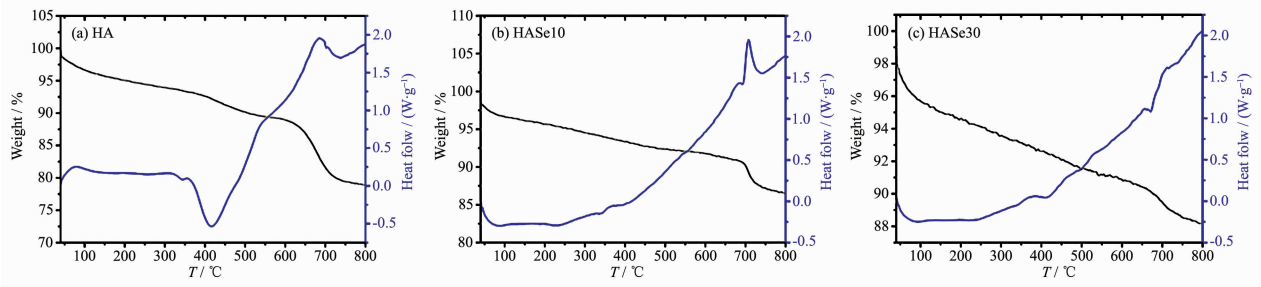

Fig.5 Thermal-gravity changes profiles of HA and HASe microspheres

2.3 *In vitro* degradation experiment

The *in vitro* degradation profile of HASe10 microspheres was monitored by immersing them into PBS (pH 3.5 or 10.5), which was incubated at 37 ℃ in a water bath with constant shaking. As shown in Fig.6, the *in vitro* degradation behavior and selenium release profiles of the HASe10 microspheres exhibit a similar feature. Fig.6a shows that the cumulative degradation percentage of the HASe10 microspheres was a proximately linear relationship over a time period of one week. The degradation curve of the HASe10 microspheres presented two stages. In no more than 76 h (0~76 h), the degradation percentage decreased with the increase of pH value from 3.5 to 10.5. After 76 h till 164 h (76~164 h), the degradation percentage increased with the increase of pH value. During one week, approximately 12.99% and 15.43% of the HASe10 microspheres were degraded in the PBS with

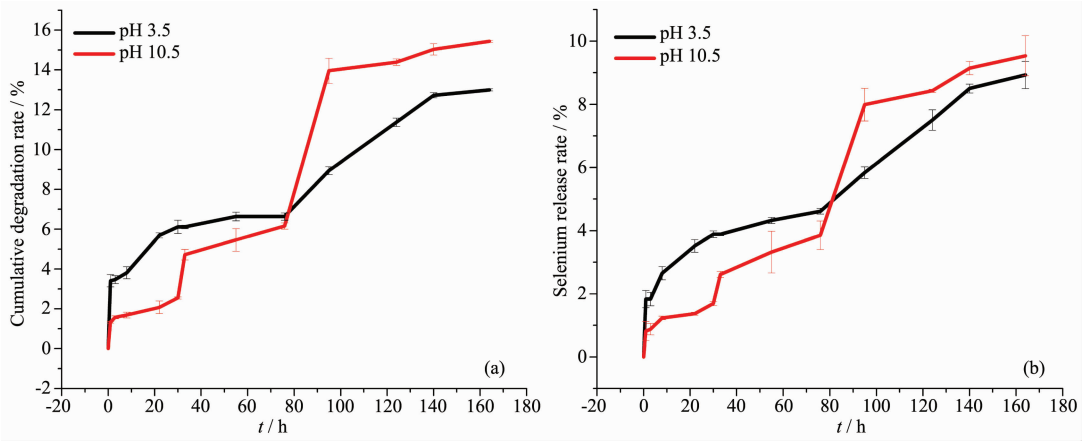

(a) Cumulative degradation rate; (b) Selenium release rate

Fig.6　*In vitro* degradation analysis of HA and HASe microspheres

a pH of 3.5 and 10.5. The cumulative degradation percentage at pH 10.5 was somewhat higher than that at pH 3.5. Although many evidences have proved the dissolution rate of the HA microspheres was faster at a lower pH value [1,14,16], in this work, the faster degradation was observed at the higher pH value. As the HASe microspheres presented sustainable biphasic degradation pattern, it is inferred that, in the initial phase, the faster dissolution of HASe nanorods of the sphere improves the degradation in the lower pH value, then the pH value of the degradable solution arises close to the neutral which slows down the degradation speed. The selenium release profile (Fig. 6b) of the HASe10 microspheres was almost similar with the degradation pattern, which exhibited a pH-responsive effect. It is speculated that, only when the spheres degrade in the buffer solution, the selenite ions could be released from it.

2.4　Drug loading and *in vitro* drug release

The amounts of Cur loaded on the HA, HASe10 and HASe30 microspheres were (0.00±0.00), (88.72±0.01) and (72.82±0.15) $mg \cdot g^{-1}$, respectively. The HASe microspheres could be used for controlling drug release because they possessed large specific surface areas, hollow porosity and good bioactivity. And our previous study about HASe nanocarriers provided certain useful information: the selenite ions doped into HA structure could cause the decreased crystallinity and increased solubility of the crystal[19]. For loading lysozyme, the HASe10 was the sole phase with the highest loading capability. The addition of selenium into HA structure seems to make this specific drug more facilely affine with the crystal, and this is the reason why drug loading efficacy of HA increased especially after elemental doping. Selenite ions itself exhibit antitumor effect on various type of carcinoma, whereas HA is employed as novel drug vehicle owing to large drug loading capacity and stable controllable release property. And the related reports[14] showed that the pure HA microspheres via hydrothermal fabrication perform excellent behavior of loading large amounts of DOX, and there is obvious effectiveness of providing useful amount of the loaded drug to the pathologic region. Thus in this view, the HASe have the potential as controlled-release carriers to load certain drugs. In this work, the UV-Vis absorption spectra of the aqueous solution containing Cur before and after drug loading were employed to evaluate the drug loading content and entrapment efficiency of HASe microspheres. The HASe10 microspheres showed an impressively highest drug entrapment efficiency of (88.72±0.06)%, meanwhile, the drug loading content was (88.72±0.01) $mg \cdot g^{-1}$, which was a relatively high value for hydroxyapatite based carriers commonly reported in the references[14]. It is obvious that the porous and hollow structure of the HASe microspheres plays a key role in providing strong adsorption for Cur molecules and thus enhancing the drug loading capacity. The excellent drug loading capacity is also attributed to the large specific surface area and

porosity. The negatively charged PSS remains in the HASe microspheres, and it could provide additional attractive force for the positively charged Cur due to the electrostatic attraction between PSS and Cur. Moreover, the negative units of OH^- and PO_4^{3-} in the hydroxyapatite structure can provide these carriers with greater affinity towards Cur molecules. The drug molecules can attach onto the HASe microspheres through hydrogen bonding interactions due to the presence of hydroxyl groups in both the drug molecules and the HASe microspheres.

The cumulative Cur release profiles of the Cur-loaded HASe microspheres in PBS are summarized in Fig.7. The drug release curve showed that, two Cur-loaded HASe microspheres (HASe10 and HASe30) had the similar tendency under PBS with pH values of 7.2±0.2. The slow release lasted for about 159 h, and Se doping amount had no significant effect on the release effect. In contrast with pure HA, the two HASe microspheres (HASe10 and HASe30) showed slower release effect. It can be visible that the release rate of Cur decreases with the addition of the dopant. There was no burst release presented in the Cur-loaded HASe microspheres, instead, they showed a slow and sustainable controlled release from beginning to the endpoint of the release test. In the PBS with pH 7.2 at 0~159 h, approximately 34.6% (1.73/5), 29.0% (1.45/5) and 27.6% (1.38/5) of loaded Cur were released from the Cur-loaded HA microspheres. Interestingly, the cumulative release curve of Cur presented an approximately linear relationship with drug release time from 0~159 h. The mechanisms about the in vitro Cur release profiles are complex. For example, Pizzoccaro et al. studied the adsorption and release behavior of benzoxaboroles on hydroxyapatite crystalline, and a rapid release pattern was got in the physiological media, which is caused by the weak binding force between the drugs and the crystals[37]. Therefore, the knowledge about the phase transformation of the HA microcarriers, desorption and diffusion of Cur, and electrostatic interaction between the carrier and drug, could provide some insights to decipher the excellent controlled-release property of the Cur-loaded HASe microspheres system.

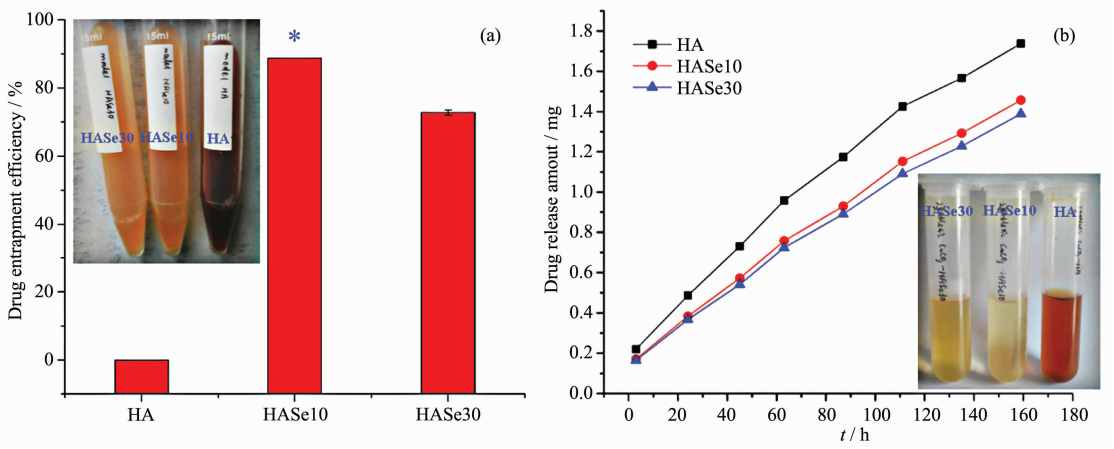

Fig.7 (a) Drug entrapment efficiency of HA and HASe microspheres; (b)Drug release amount of Cur from HA and HASe microspheres

2.5 Hemolysis assay

The whole blood from healthy individuals was applied to test the cytotoxicity and hemolysis properties of the HASe microspheres. Table 2 summarizes the tested data. From the results, the HASe10 microspheres exhibit less toxic to the blood cells than the other two samples (HA and HASe30), and it could hardly cause hemolysis of the red blood cells (RBC), because the content of the hemoglobin was the lowest among them. On contrary, the HA and HASe30 group increased the amount of the HGB, which implied they could cause weakly hemolytic response. There was no significant difference in WBC and RBC number among three samples, but the value of the PLT in the

two HASe samples was higher than pure HA microspheres, one of the reasonable assumptions is that, it is possible to split certain platelet by the HASe microspheres, and the PLT fragment attaches onto the surface of the nanorods units of the microspheres, therefore the recorded value via the equipment arises. This also indicates the two HASe microspheres show mildly toxic to the PLT. Although the value of PLT was high, it was in the normal range. And other parameters presented no statistical difference. Combined the components of the microspheres with the hemolysis analysis, the synthetic HASe10 microspheres could be an effective carrier for drug delivery. Many reports confirm the excellent biocompatibility of HA, because it is the main inorganic component of human bone and teeth. Selenium itself is a nutritional trace element, requisite for the growth of many cells. HASe nanoparticles were synthesized successfully, and could load lysozyme for controlled release *in vitro*. In this work, the HASe microspheres similarly show large Cur loading capacity and slowly stable release effect. And it possesses no hemolytic toxicity and cytotoxicity to the normal blood cells. Therefore, it has great potentials in the aspect of biomedical application, especially as an effective microcarrier to load drugs for the oncotherapy of bone tumors.

Table 2　Hemolysis properties of the HA and HASe microspheres*

	HA	HASe10	HASe30
N_{WBC} / L^{-1}	$(6.24\pm1.07)\times10^9$	$(5.78\pm1.15)\times10^9$	$(6.04\pm1.57)\times10^9$
N_{RBC} / L^{-1}	$(4.27\pm0.14)\times10^{12}$	$(3.93\pm0.09)\times10^{12}$	$(4.35\pm0.42)\times10^{12}$
c_{HGB} / ($g\cdot L^{-1}$)	123.67±7.57	114.67±3.21	129.67±13.65
HCT / %	39.90±2.00	36.87±1.37	40.23±3.87
MCV / fL	93.50±1.78	93.80±5.17	92.50±0.52
MCH / pg	29.00±0.87	29.17±1.15	29.77±0.38
MCHC / ($g\cdot L^{-1}$)	310.00±3.61	311.00±6.08	322.00±3.61
N_{PLT} / L^{-1}	$(147.67\pm20.60)\times10^9$	$(205.33\pm74.04)\times10^9$	$(209.67\pm15.95)\times10^9$
RDW-SD /fL	41.83±0.12	40.77±2.97	41.47±0.31
RDW-CV / %	12.57±0.29	12.23±0.35	12.73±0.12
PDW / fL	18.07±1.76	13.03±1.68	14.23±2.16
MPV / fL	13.17±0.12	11.33±0.81	11.70±0.87
P-LCR / %	49.43±0.97	35.60±6.99	38.13±6.45
PCT / %	0.20±0.03	0.23±0.07	0.25±0.02
N_{NEUT} / L^{-1}	$(4.16\pm0.96)\times10^9$	$(3.56\pm0.63)\times10^9$	$(3.52\pm1.41)\times10^9$
N_{LYMPH} / L^{-1}	$(1.74\pm0.15)\times10^9$	$(1.81\pm0.53)\times10^9$	$(2.11\pm0.25)\times10^9$
N_{MONO} / L^{-1}	$(0.29\pm0.04)\times10^9$	$(0.28\pm0.03)\times10^9$	$(0.29\pm0.01)\times10^9$
N_{EO} / L^{-1}	$(0.04\pm0.01)\times10^9$	$(0.11\pm0.04)\times10^9$	$(0.08\pm0.03)\times10^9$
N_{BASO} / L^{-1}	$(0.01\pm0.01)\times10^9$	$(0.02\pm0.01)\times10^9$	$(0.04\pm0.01)\times10^9$
R_{NEUT} / %	66.13±4.48	61.80±2.66	57.03±7.85
R_{LYMPH} / %	28.17±3.06	31.00±3.18	35.97±6.43
R_{MONO} / %	4.80±1.56	4.93±1.27	5.10±1.37
R_{EO} / %	0.70±0.10	1.97±0.64	1.27±0.15
R_{BASO} / %	0.20±0.17	0.30±0.10	0.63±0.25

* WBC: white blood cells; RBC: red blood cells; HGB: hemoglobin; HCT: hematocrit; PCT: platelet hematocrit; MCV: mean corpuscular volume; MCH: mean corpuscular hemoglobin; MCHC: mean corpuscular hemoglobin concentration; RDW: red blood cell volume distribution width; RDW-SD: red blood cell volume distribution width-standard deviation; PLT: platelet; MPV: mean platelet volume; PCT: platelet hematocrit; PDW: platelet volume distribution width; P-LCR: platelet-large cell ratio; NEUT: neutrophils; LYMPH: lymphocytes; MONO: monocytes; EO: eosinophils; BASO: basophiles

2.6 Cytotoxicity assay

The Fig.8a shows the changes of the cell viability of the cancerous SOSP-9607 cells and the normal RAW-264.7 cells after treated by these microspheres. There was significant difference between the two types of cell line. Seemingly, the HASe microspheres presented cell type specific effect: They could promote the growth of normal RAW-264.7 cells due to the greatly increased cell viability compared with the control group; simultaneously, they exhibited inhibitory effect on the growth of the cancerous SOSP-9607 cells due to the decreased cell viability compared with the control group. From the above data, it is inferred that, the HASe microspheres have no obvious toxicity to normal cells, but greatly toxic effect to cancerous cells. And selenium doped into the HA structure increases the inhibitory efficacy on the growth of cancerous SOSP-9607 cells. The effect was also confirmed in the migration test (Fig.8b): in the control group, many cells had the ability to migrate, and they could cluster together to form cell colony; in the HASe group, it was visible that certain living cells scattered in the bottom of the plate, but many cells died and the cellular compartment became wider. The above effect was slightly similar with the Sr doped hydroxyapatite nanocrystals, which could enhance the osteogenic and inhibit the osteoclastic effect [38]. The synthetic HASe microspheres could improve the growth of normal cells, whilst inhibiting the growth of the cancerous cells. Such dual-functional effect could be used to design the multifunctional bone grafts in the therapy of the bone cancer.

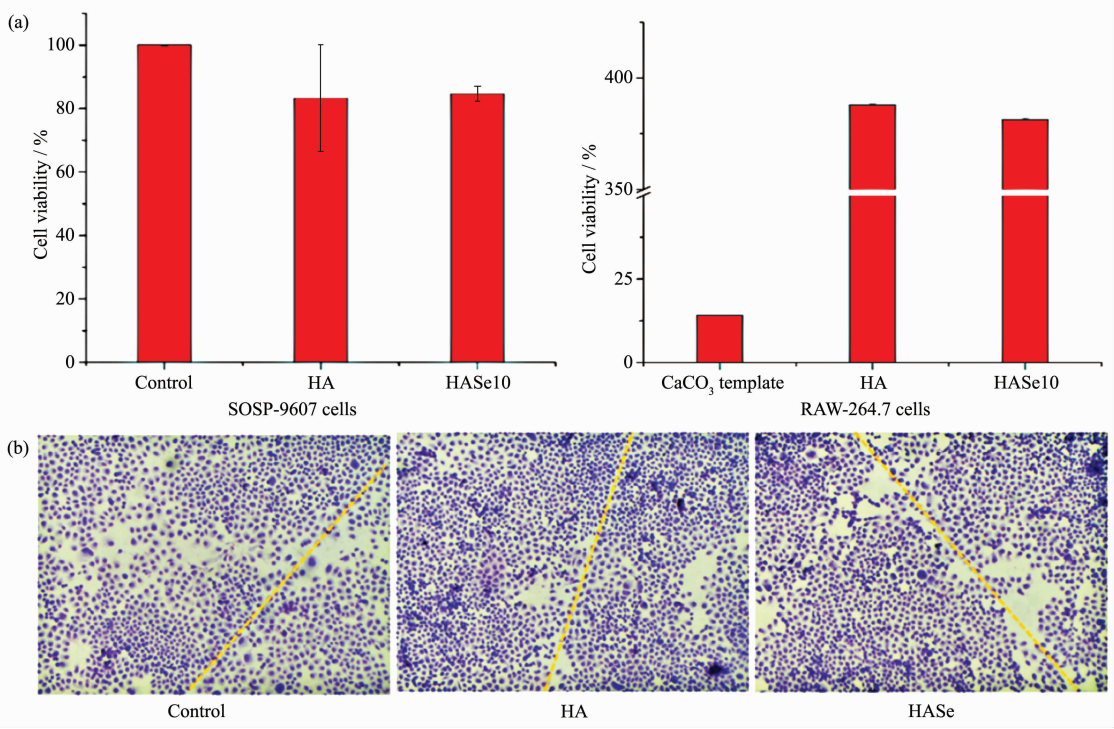

Line inserted in (b) is the initial scratch during the test

Fig.8 Cytotoxicity analysis of the HA and HASe microspheres: (a) cell viability of the cancerous SOSP-9607 and normal RAW-264.7 cells; (b) cell density of the cancerous SOSP-9607 cells

3 Conclusions

The HASe microspheres have been successfully synthesized by a hydrothermal method using the vaterite $CaCO_3$ as the sacrificial template. The morphology and size of vaterite $CaCO_3$ play a key role in regulating the structure of the HASe microspheres. The HASe microspheres have a size distribution from 0.8 to 1.6 μm, with an average diameter of about 1.0 μm. The wall of HASe microspheres is constructed with subtle units of hydroxyapatite nanorods with an average length of 150 nm and an average width of 20

nm. The synthetic strategy of the microspheres is rapid, highly efficient, energy-saving and environmentally friendly. This work explored the potential application of the HASe microspheres for drug loading and controlled release. The prepared HASe microspheres display a high drug loading capacity and sustained-controlled release behavior for Cur. Moreover, the HASe microspheres controlled release system shows no hemolytic and cytotoxic to the blood cells. Cell co-culture testifies that the HASe microspheres could inhibit the proliferation of the cancerous SOSP-9607 cells, but promote the growth of normal RAW-264.7 cells. The dual-effect indicates that HASe microspheres are promising for applications in various biomedical fields such as drug delivery system and oncotherapy. From the point of view, HASe10 microspheres could be a novel micro-carrier for the treatment of bone related diseases such as osteosarcoma.

Acknowledgements: We sincerely thank for the help of Dr. XIANG Hui-Yao at the first college of clinical medical science of China Three Gorges University for the constructive suggestion and data analysis about this study. This work was supported by National Natural Science Foundation of China (Grant No. 81602559) and by Youth Science Fund Program of China Three Gorges University (Grant No. 1115064).

References:

[1] Maia A L, Cavalcante C H, Souza M G, et al. *Nucl. Med. Commun.*, 2016,37:775-782

[2] ZU Qing-Xia(朱庆霞), LI Ya-Ming(李亚明), HAN Dan(韩丹). *Journal of Functional Materials*(功能材料), **2018**,**49**(2): 2130-2135

[3] Raina D B, Isaksson H, Hettwer W, et al. *Sci. Rep.*, **2016**,**6**: 26033-26045

[4] Hayashi M, Aoshi T, Kogai Y, et al. *Vaccine*, **2016**,**34**:306-312

[5] Wang X P, Li X, Ito A, et al. *Chem. Commun.*, **2016**,**52**: 7078-7081

[6] Bertran O, Revilla-Lopez G, Casanovas J, et al. *Chemistry*, **2016**,**22**:6631-6636

[7] Ilie A, Ghitulica C, Andronescu E, et al. *Int. J. Pharm.*, **2016**, **510**:501-507

[8] Jafari S, Maleki-Dizaji N, Barar J, et al. *Eur. J. Pharm. Sci.*, **2016**,**91**:225-235

[9] Chen X, Yang B, Qi C, et al. *Dalton Trans.*, **2016**,**45**:1648-1656

[10]Kamitakahara M, Ohtoshi N, Kawashita M, et al. *J. Mater. Sci.*: *Mater. Med.*, **2016**,**27**:93-99

[11]Li D, Huang X, Wu Y, et al. *Biomater. Sci.*, **2016**,**4**:272-280

[12]Benedetti M, De Castro F, Romano A, et al. *J. Inorg. Biochem.*, **2016**,**157**:73-79

[13]Wang Y, Hao H, Zhang S. *Mater. Sci. Eng. C*: *Mater. Biol. Appl.*, **2016**,**61**:545-552

[14]Lai W, Chen C, Ren X, et al. *Mater. Sci. Eng. C*: *Mater. Biol. Appl.*, **2016**,**62**:166-172

[15]Yang P P, Quan Z W, Li C X, et al. *Biomaterials*, **2008**,**29**: 4341-4347

[16]Xie G P, Sun J A, Zhong G R, et al. *J. Mater. Sci.*: *Mater. Med.*, **2010**,**21**:1875-1880

[17]Yang H, Hao L J, Zhao N R, et al. *CrystEngComm*, **2013**, **15**:5760-5763

[18]Wan Y Z, Wu C Q, Zuo G F, et al. *Mater. Chem. Phys.*, **2015**,**156**:238-246

[19]Ma J, Wang Y, Zhou L, et al. *Mater. Sci. Eng. C*: *Mater. Biol. Appl.*, **2013**,**33**:440-445

[20]Wang Y H, Hao H, Liu H M, et al. *Adv. Healthcare Mater.*, **2015**,**4**:1813-1818

[21]Qi C, Zhu Y J, Lu B Q, et al. *Chem. Eur. J.*, **2013**,**19**:5332-5341

[22]Wang Q, Huang W H, Wang D P, et al. *J. Mater. Sci.*: *Mater. Med.*, **2006**,**17**:641-646

[23]Yu Y D, Zhu Y J, Qi C, et al. *J. Colloid Interface Sci.*, **2017**,**496**:416-424

[24]Fu H L, Rahaman M N, Day D E, et al. *J. Mater. Sci.*: *Mater. Med.*, **2011**,**22**:579-591

[25]Feng D S, Shi J, Wang X J, et al. *RSC Adv.*, **2013**,**3**:24975-24982

[26]Zhong Q, Li W, Su X, et al. *Colloids Surf. B*, **2016**,**143**:56-63

[27]Xiao W, Bal B S, Rahaman M N. *Mater. Sci. Eng. C*: *Mater. Biol. Appl.*, **2016**,**60**:324-332

[28]Xiao Q, Zhou K, Chen C, et al. *Mater. Sci. Eng. C*: *Mater. Biol. Appl.*, **2016**,**69**:1068-1074

[29]Ma M Y, Zhu Y J, Li L, et al. *J. Mater. Chem.*, **2008**,**18**: 2722-2727

[30]Ye F, Guo H F, Zhang H J, et al. *Acta Biomater.*, **2010**,**6**: 2212-2218

[31]Qi C, Zhu Y J, Lu B Q, et al. *J. Mater. Chem.*, **2012**,**22**: 22642-22650

[32]Pulido-Moran M, Moreno-Fernandez J, Ramirez-Tortosa C, et al. *Molecules*, **2016**,**21**:264-285

[33]Sarika P R, Nirmala R J. *Mater. Sci. Eng. C: Mater. Biol. Appl.*, **2016**,**65**:331-337

[34]Chen P, Wang H, Yang F, et al. *J. Cell Biochem.*, **2017**,**118**:74-81

[35]Sahebkar A. *Integr. Cancer Ther.*, **2016**,**15**:333-334

[36]Shi J, Qi W, Du C, et al. *J. Appl. Polym. Sci.*, **2013**,**129**:577-584

[37]Pizzoccaro M A, Nikel O, Sene S, et al. *Acta Biomater.*, **2016**,**41**:342-350

[38]DAI Zhao(代钊), WANG Da-Lin(汪大林). *Chinese Journal of Tissue Engineering Research*(中国组织工程研究), **2018**, **22**(6):938-944